$[Ru^{V}(NCN\text{-}Me)(bpy)(=O)]^{3+}$ Mediates Efficient C–H bond Oxidation from NADH Analogs in Aqueous Media rather than Water Oxidation

Jully Patel, [a] Karunamay Majee, [a] Ejaz Ahmad, [a] Koji Tanaka, *, [b] and Sumanta Kumar Padhi *, [a]

[a]Department of Applied Chemistry, Indian School of Mines, Dhanbad, 826 004, Jharkhand, India
[b]Institute for Integrated Cell-Material Sciences, Kyoto University, Advanced Chemical Technology Center in Kyoto (ACT Kyoto) jibuchou 105, Fushimiku, Kyoto 612-8374, Japan

*E-mails: padhi.sk.ac@ismdhanbad.ac.in
And
koji.tanaka@icems.kyoto-u.ac.jp

Supporting Information

Experimental Methods

Instrumentation and Materials: All the manipulations were carried out using standard Schlenk techniques under nitrogen atmosphere. Diethyl ether, dichloromethane, acetonitrile, acetone, ethanol and hexane were dried, degassed and stored under nitrogen atmosphere prior to use.

NMR Spectroscopy: NMR spectra were recorded on a NMR spectra were recorded on a BRUKER AvII-400 MHz NMR spectrometer (400 MHz for ^{1}H and 100.62 MHz for ^{13}C) at room temperature.

EPR Spectroscopy: The EPR spectra at 77 K were measured with a JEOL X-band spectrometer (JES-FA200) using liquid nitrogen dewar. The g values were calibrated precisely with an Mn^{2+} marker which was used as a reference. X-band frequency 9.44 GHz, Microwave power was 1.0 mW and the amplitude was 0.1 mT.

Mass Spectroscopy: High resolution ESI mass spectra were recorded on a Waters UPLC TQD (ESI MS and APCI MS).

Optical Spectra: The UV-vis-NIR spectra were recorded on a Shimadzu UV-1800 and Cary 5000 UV-vis-NIR scanning spectrophotometer.

Gas evolution: The O_2 evolution has been carried out was based upon the manometry results. In this case 2 μmol of complex and 100 equiv. of CAN added in 2 mL of pH~1 triflic acid. A differential pressure manometer of (Testo 521 with range 0-100 hPa and accuracy 0.2%) used to measure the O_2 pressure.

Cyclic Voltammetry: Electrochemical measurements were carried out under nitrogen atmosphere using an ALS/Chi model 660D electrochemical analyzer at 25°C at a scan rate of 100 mV in water with a complex concentration of 0.5 mM. The working, auxiliary and reference electrodes were AS Glassy Carbon electrode, platinum wire, and Saturated Calomel Electrode (SCE), respectively. Both Cyclic voltammetry and controlled-potential electrolysis were carried out under nitrogen atmosphere. The complexes were dissolved in a degassed solvent containing the necessary amount of the supporting electrolyte. Single buffer of H_3PO_4 was used with the sequential addition of KOH. The minimum ionic strength of 0.1 M was maintained with the addition of KPF_6 into the aqueous solution. The regions at pH

2.9 and 10.5 were cross verified by phthalate buffer and borate buffer several times using a constant ionic strength and the data were added to the respective potentials.

Controlled Potential Electrolysis:

An H-type electrolysis cell which consists of two compartments: the working (glassy carbon plate, 1 cm^2) and the counter (platinum plate) electrodes were separated by an porous frit was used. Both Cyclic voltammetry and controlled-potential electrolysis were carried out under nitrogen atmosphere. The solution was of 5 mL. The bulk electrolysis were carried out in support of electron transfer reactions at 1.10 V and 0.95 V *vs.* SCE and pH≈1.62. The calculated electrons were respectively 3 electron and two electron oxidation at potentials 1.10 V and 0.95 V *vs.* SCE. Prior to the pre-electrolysis was carried out for 30 mins in pH≈1.62 phosphate buffer, at 1.10 V *vs.* SCE. The controlled potential electrolysis consumed a total charge of 7.250 x 10^{-2} C, for a complex concentration of 0.05 mM (0.0002 g). The resulting number of electrons involved in the oxidation process was calculated to be ≈ 3.0. At 0.95 V the total charge consumed was 4.376 x 10^{-2} C, for a complex concentration of 0.05 mM (0.0002 g). The resulting number of electrons involved in the oxidation process was calculated to be ≈ 2.0 excluding the resedual charge during the pre-electrolysis. The coulometric results confirms the presence of Ru^{VI}=O state at 1.01 V vs. SCE since the complex 1 exists as Ru^{III}-OH_2 at pH≈1 phosphate buffer.

X-ray crystallographic analysis: The X-ray crystallographic data for the complexes were collected using Bruker SMART APEX-CCD diffractometer with Mo Kα radiation (λ = 0.71073 Å). The intensity data were corrected for Lorentz and polarization effects and empirical absorption corrections was applied using SAINT program.[1] The structure was solved by direct methods using SHELXS-97 and non-hydrogen atoms located from the difference Fourier maps were refined anisotropically by full-matrix least-squares on F^2 using SHELXL-97.[2] The hydrogen atoms were included in the calculated positions and refined isotropically using a riding model.

Synthetic Procedures:

Synthesis of [Ru(NCN-Me)(bpy)(I)]PF_6 (**2**).

To a solution of (0.300 g, 0.62 mmol) of [Ru(bpy)$(DMSO)_2Cl_2$] in 50 mL of ethanol was added with (0.313 g, 1.24 mmol) of $AgPF_6$ (0.097 g, 0.62 mmol) and allowed to stir about 1 h at 80 °C. A dark orange color solution formed along with the off-white precipitates of AgCl. The precipitates of AgCl were filtered through celite, with sufficient ethanol and collected in a 15 mL round bottom flask. To the above reaction mixture NCN-Me is N-methyl-3,5-di(2-pyridyl)pyridinium iodide (0.232 g, 0.62 mmol) was added and refluxed at 80 °C for 12 h. The crude product evaporated in *vacuo* and purified by column chromatography on basic alumina using CH_2Cl_2/EtOH by 99:1 (v/v) ratio to give [Ru^{II}(NCN-Me)(bpy)(I)](PF_6) of (0.230 g, 0.30 mmol, Yield: 48 %). HRMS (ESI): Calc. for $C_{26}H_{21}IN_5Ru$ [Ru^{II}(NCN-Me)(bpy)(I)]$^+$ *m/z* 631.99 found 631.87. Calc. for $C_{26}H_{21}F_6IN_5PRu$: %C 40.22, %H 2.73, %N 9.02; found %C 40.32, %H 2.76, %N 9.08. The 400 MHz ^{1}H NMR (δ, (*J*, Hz), Acetone-D_6): 4.47(3H, s), 6.83 (1H, t, 4.4), 7.02 (1H, d, 7.0), 7.15 (2H, t, 7.3), 7.65 (1H, t, 7.8), 7.86 (2H, t, 7.7), 7.98 (2H, d, 3.39), 8.00 (1H, t, 2.3), 8.14 (3H, m), 8.50(1H, d, 8.1), 8.88(1H, d, 8.2), 9.04 (2H, s), 10.75(1H, d, 1.6)**.** Suitable orange color single crystals of [Ru(NCN-Me)(bpy)(I)]PF_6 (**2**) for X-ray obtained from diethyl ether vapor diffusion to the solution of **2** in acetone.

Synthesis of [Ru(NCN-Me)(bpy)(OH_2)](PF_6)$_2$ (**1**)

A Solution of **2** (0.200 g, 0.26 mmol) in a 100 mL round bottom flask containing 30 mL of acetone/H_2O (4:1 v/v) was purged under nitrogen for 30 mins and was directly added with $AgPF_6$ (0.065 g, 0.26 mmol) the solution left to stir for 1 h at 55 °C. A pale yellow precipitate of AgI filtered through celite. The filtrate was evaporated on *vacuuo* to a minimum volume and added with saturated aqueous KPF_6 solution, an orange color precipitate (0.150 g, 0.18 mmol, Yield: 69 %) was collected under centrifugation followed by washing with H_2O and dried over P_2O_5. Dark orange color single crystals suitable for X-ray grown from the aqueous solution by slow evaporation method. HRMS (ESI): Calc. for $C_{26}H_{23}F_6N_5OPRu$ ([Ru^{II}(NCN-Me)(bpy)(OH_2)]PF_6)$^+$, *m/z* 668.06 found 668.11. Calc. for $C_{26}H_{41}F_{12}N_5O_{10}P_2Ru$: %C 32.04, %H 4.24, %N 7.19; found %C 32.07, %H 4.21, %N 7.13. The 400 MHz ^{1}H NMR (δ, (*J*, Hz), Acetone-D_6): 4.48 (3H, s), 6.97(1H, d, 5.4), 7.31 (2H, t, 9.1), 7.65(1H, t, 8.5), 8.05 (4H, m), 8.17 (1H, t, 8.0), 8.56 (4H, d, m), 8.98 (1H, d, 8.2), 9.17 (2H, s), 9.87 (1H, d, 5.2). The 100.62 MHz ^{13}C NMR (δ, Acetone-D_6): 47.46, 121.79, 123.91, 124.31, 124.98, 126.34, 128.30, 131.21, 136.21, 136.82, 137.96, 144.77, 146.13, 154.35, 154.53, 154.59, 159.43, 164.26 and 236.79.

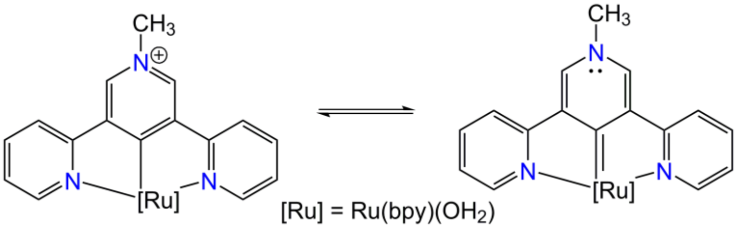

Scheme S1. Dynamic equilibrium in N-heterocyclic carbene (NHC) form of coordinated NCN-Me.

NMR Spectra:

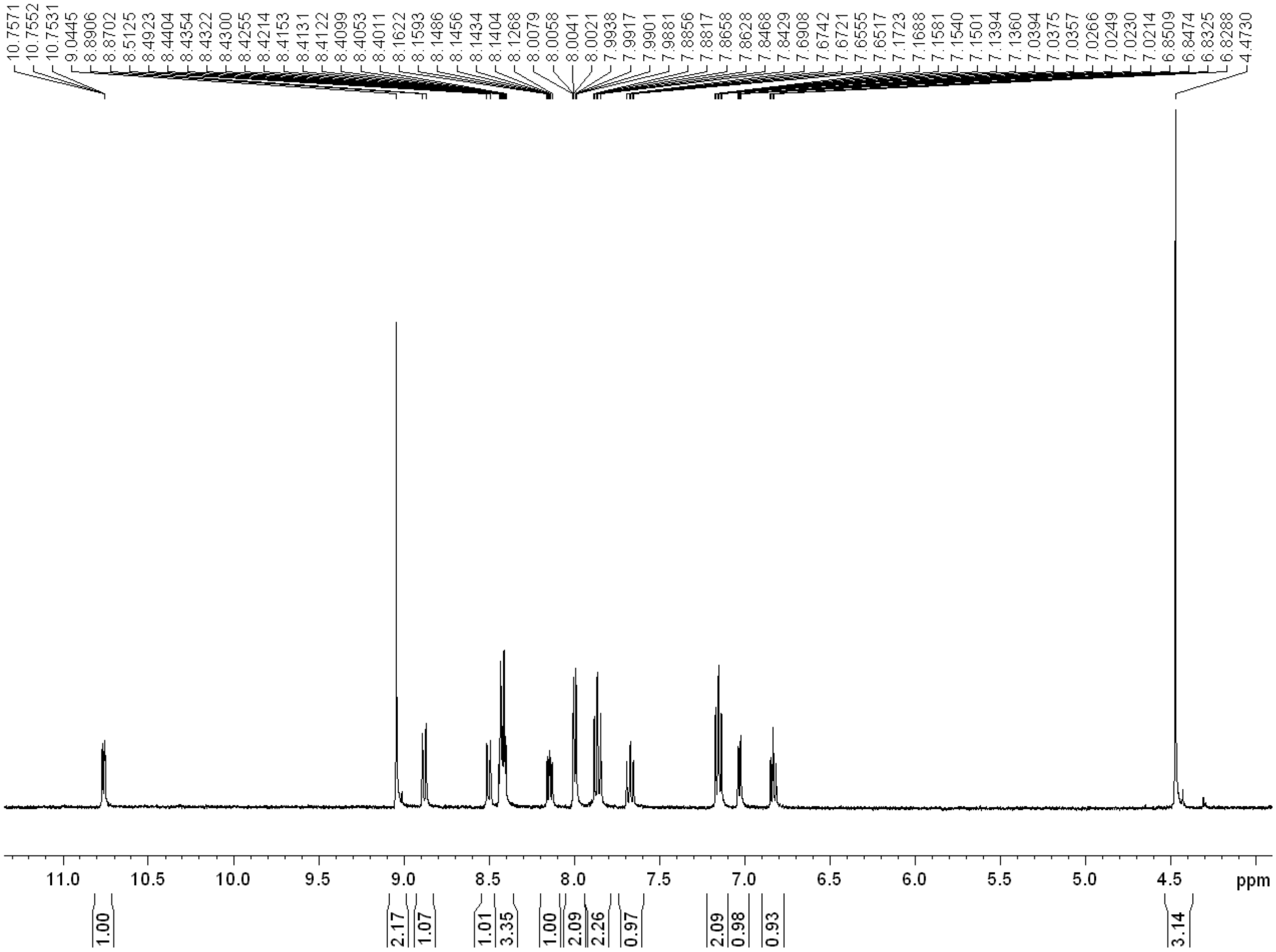

Figure S1. ^1H NMR of **2** in Acetone-D_6.

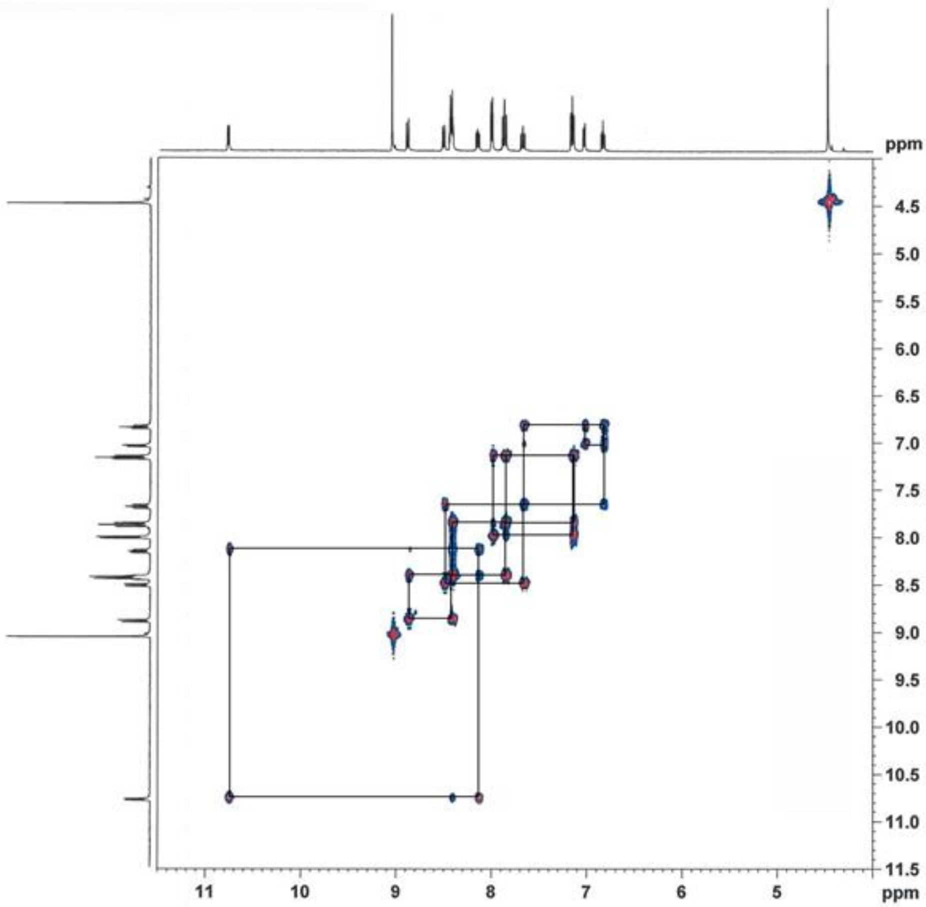

Figure S2. ^{1}H-COSY NMR of **2** in Acetone-D_6.

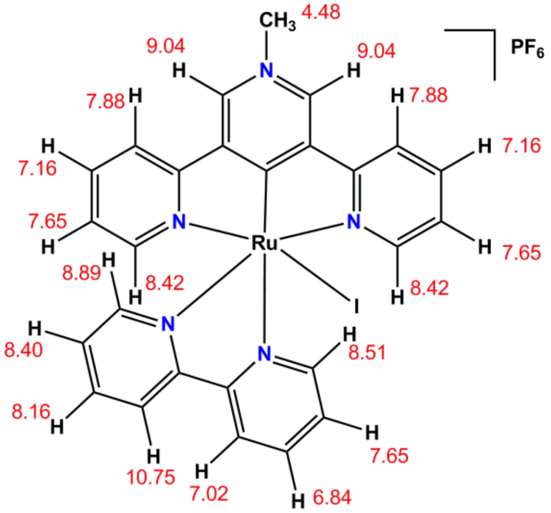

Figure S3. ^{1}H NMR assignment in **2.**

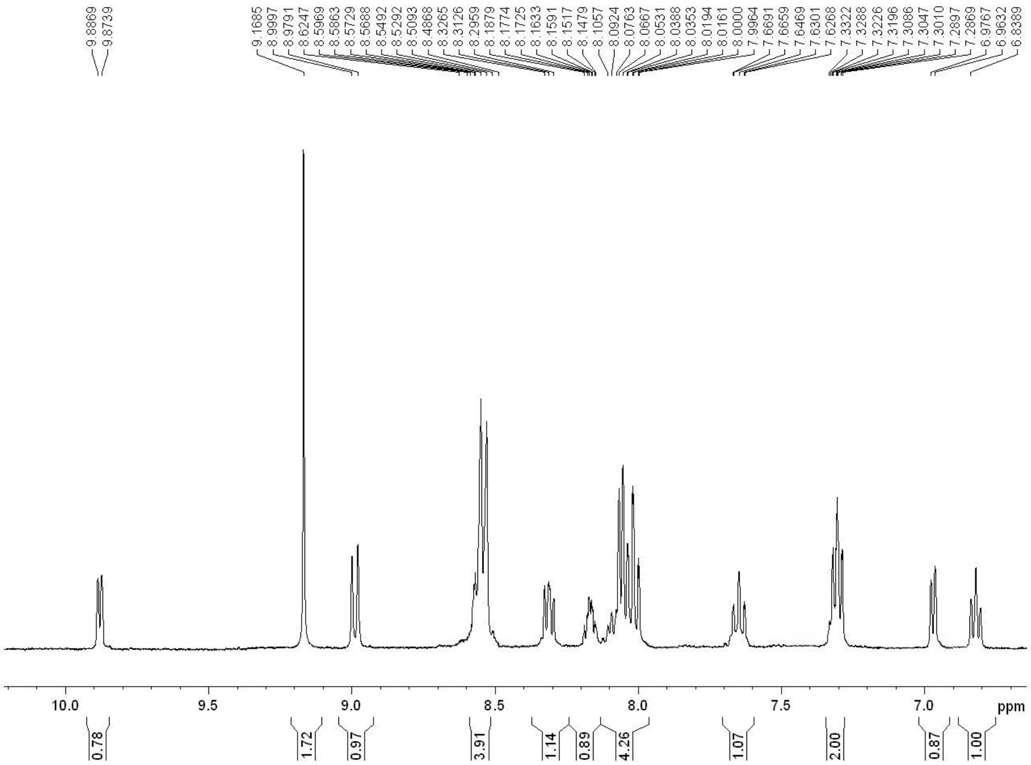

Figure S4. ^{1}H NMR of [Ru(NCN-Me)(bpy)(OH$_2$)](PF$_6$)$_2$ (**1**) in Acetone-D$_6$.

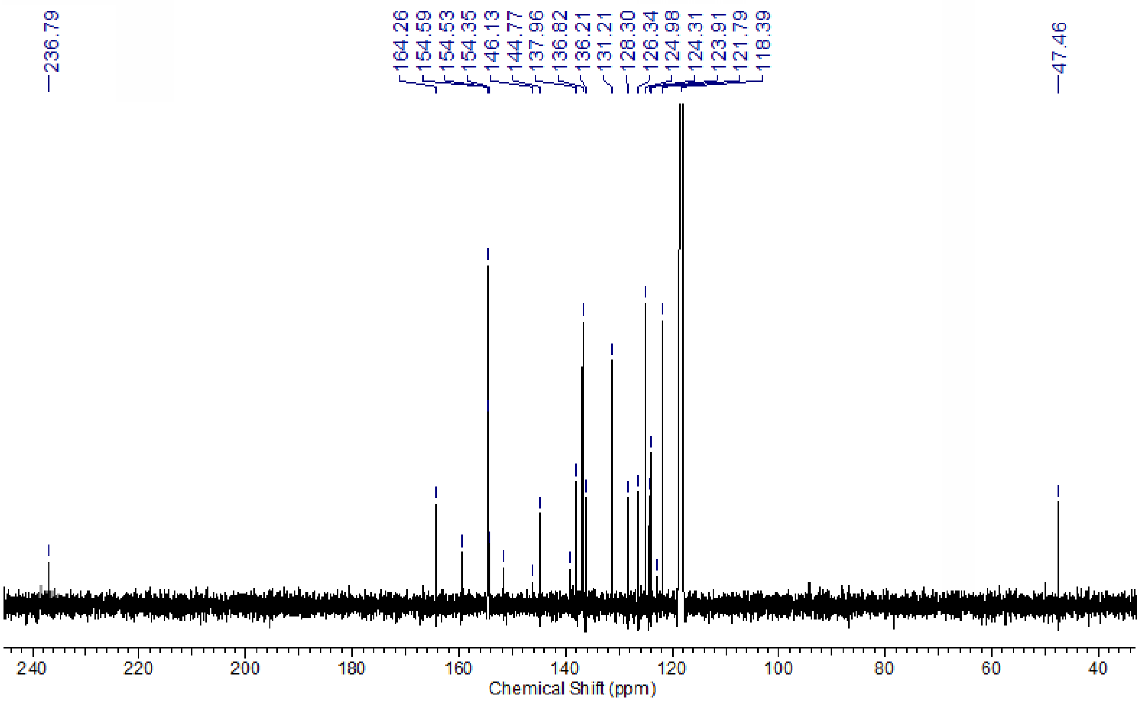

Figure S5. ^{13}C NMR of [Ru(NCN-Me)(bpy)(OH$_2$)](PF$_6$)$_2$ (**1**) in Acetone-D$_6$.

ESI Mass Spectra:

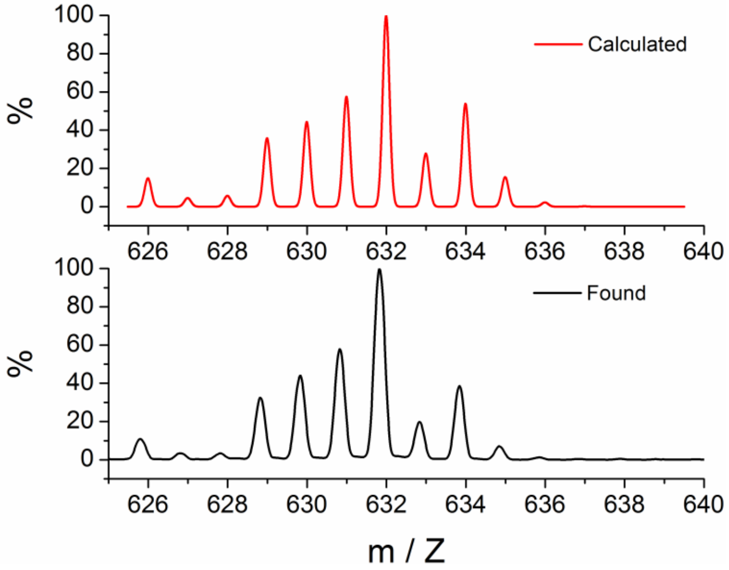

Figure S6. ESI mass of [Ru(NCN-Me)(bpy)(I)]PF_6 in CH_3CN.

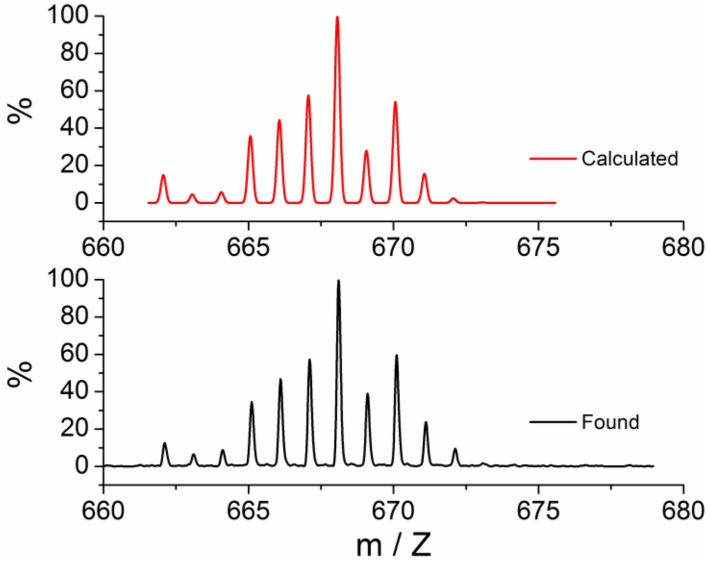

Figure S7. ESI mass of [Ru(NCN-Me)(bpy)(OH_2)]$(PF_6)_2$ in H_2O.

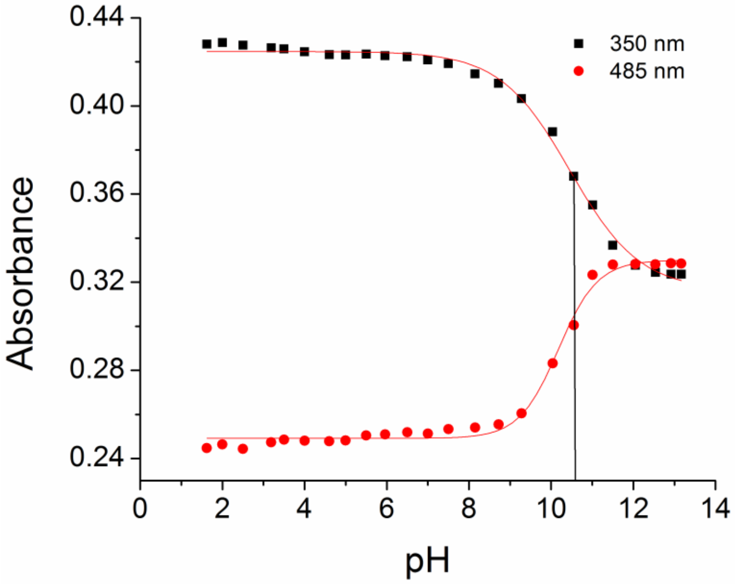

Figure S8. Absorbance *vs.* pH profile of 0.05 mM $[Ru(NCN\text{-}Me)(bpy)(OH_2)](PF_6)_2$ (**1**) in phosphate buffer.

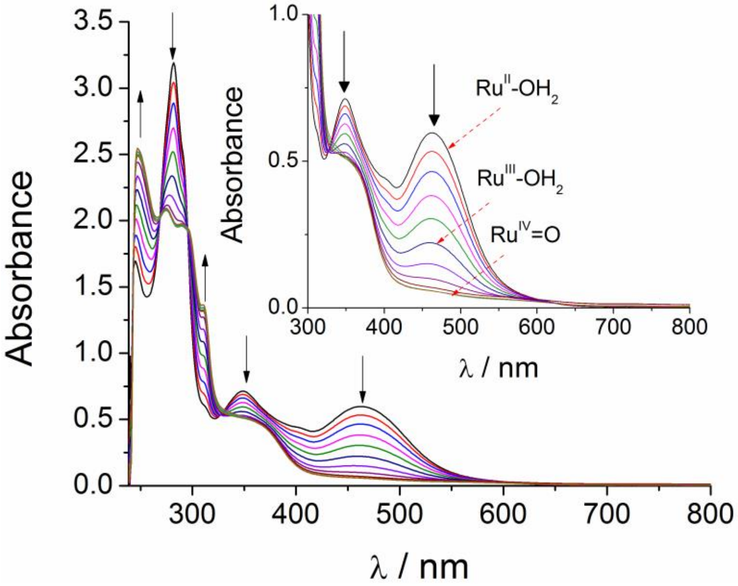

Figure S9. Change in absorbance of 0.05 mM $[Ru(NCN\text{-}Me)(bpy)(OH_2)](PF_6)_2$ (**1**) in pH~1 HNO_3 with the addition of Ce^{IV} iteratively.

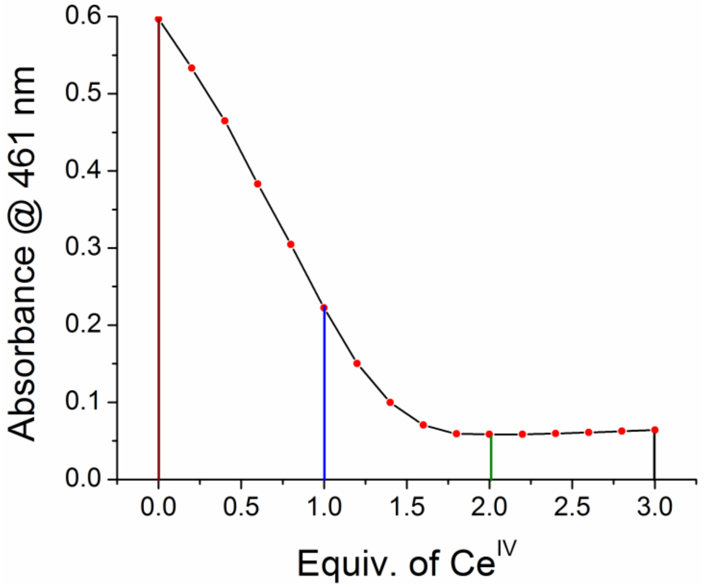

Figure S10. Absorbance *vs.* equiv. of Ce^{IV} profile of $[Ru(NCN\text{-}Me)(bpy)(OH_2)](PF_6)_2$ (**1**).

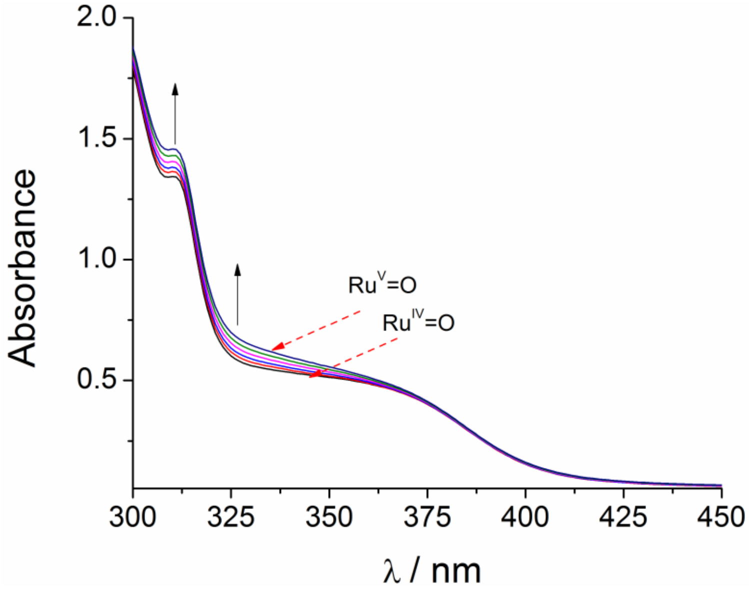

Figure S11. UV-vis spectra of different species obtained during titration with Ce^{IV} in pH~1 HNO_3.

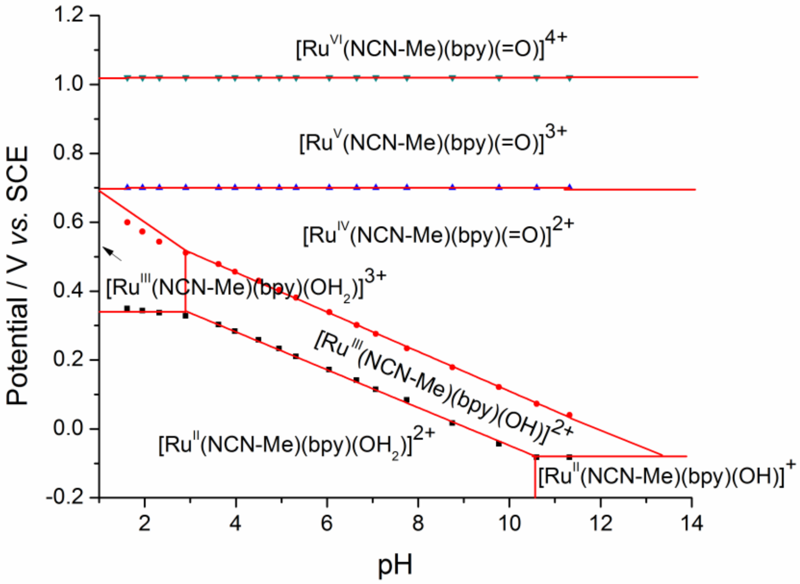

Figure S12. Pourbaix of 0.5mM [Ru^{II}(NCN-Me)(bpy)(OH$_2$)]$^{2+}$ (**1**) in phosphate buffer.

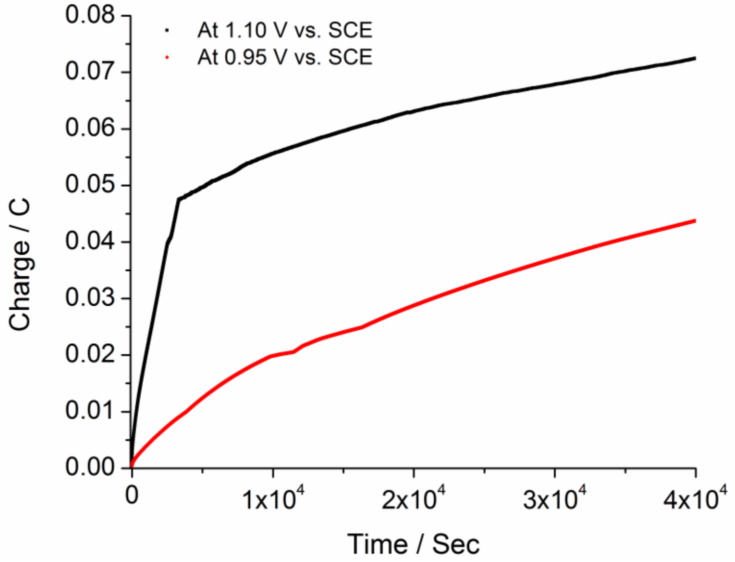

Figure S13. Controlled potential electrolysis of complex **1** at 1.10 V and 0.95 V *vs.* SCE and pH≈1.62.

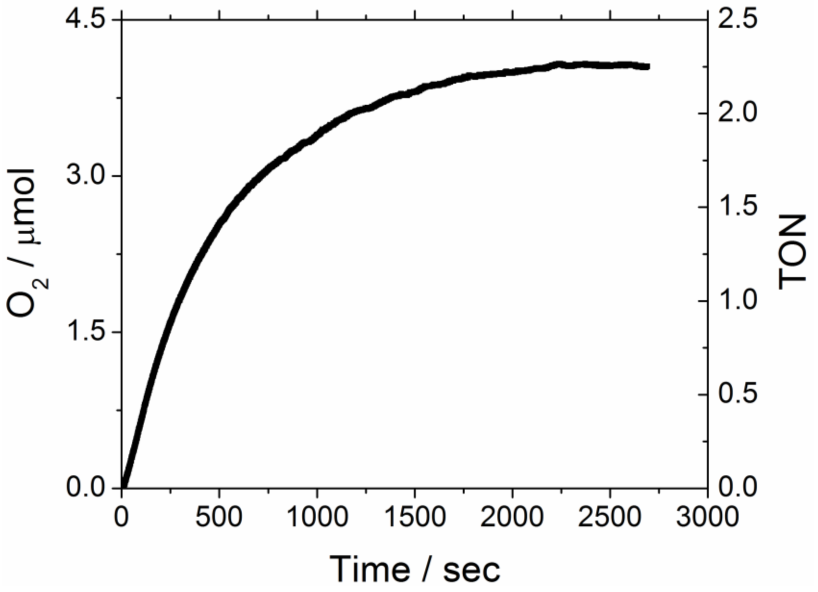

Figure S14. O_2 evolution by 1 mM of $[Ru^{II}(NCN\text{-}Me)(bpy)(OH_2)]^{2+}$ (**1**) in pH~1 triflic acid and 100 mM of CAN.

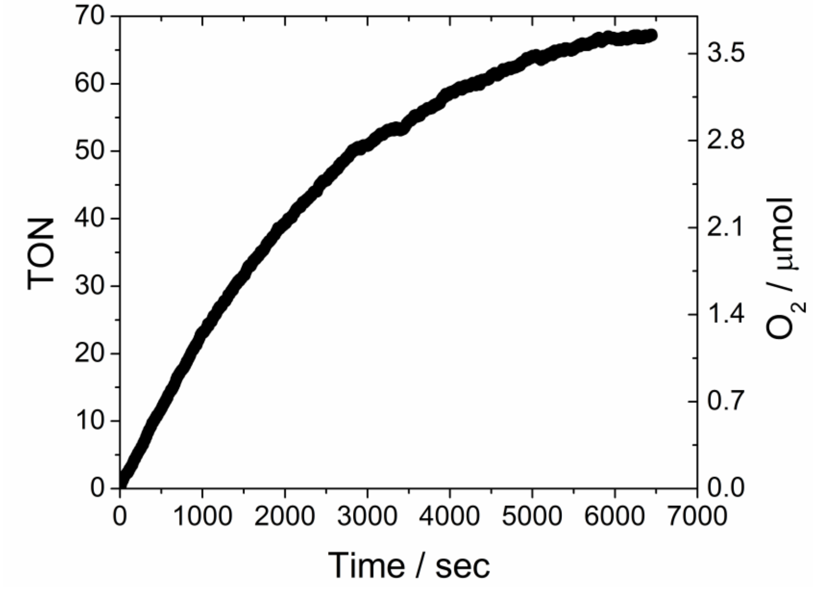

Figure S15. O_2 evolution by 0.03 mM of $[Ru^{II}(NCN\text{-}Me)(bpy)(OH_2)]^{2+}$ (**1**) in pH~1 triflic acid and 25 mM of CAN.

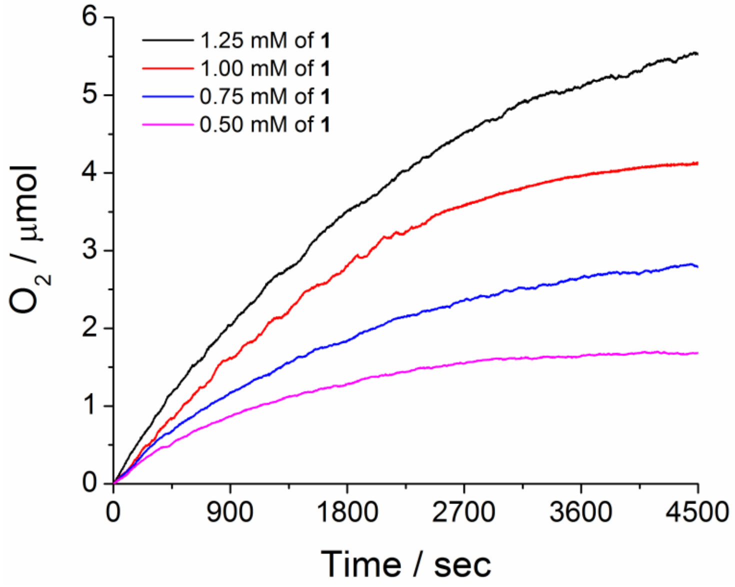

Figure S16. O_2 evolution by various concentration of $[Ru^{II}(NCN\text{-}Me)(bpy)(OH_2)]^{2+}$ (**1**) in pH~1 triflic acid and 100 mM of CAN.

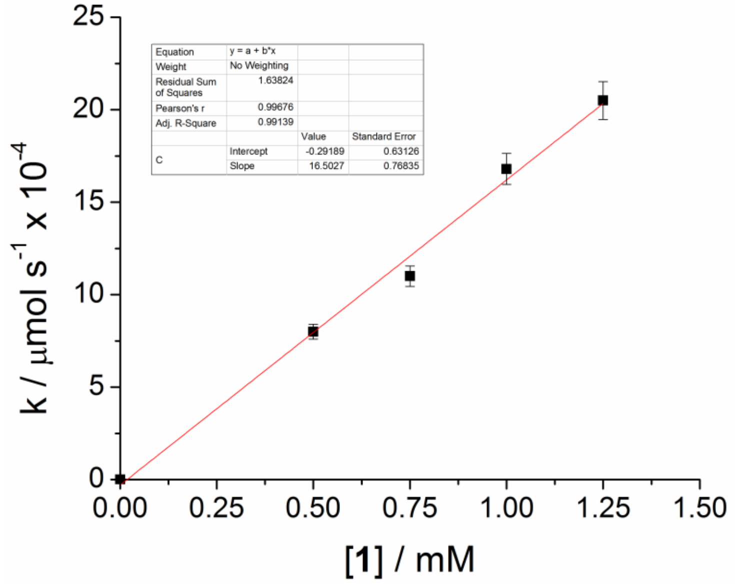

Equation	y = a + b*x		
Weight	No Weighting		
Residual Sum of Squares	1.63824		
Pearson's r	0.99676		
Adj. R-Square	0.99139		
		Value	Standard Error
C	Intercept	-0.29189	0.63126
	Slope	16.5027	0.76835

Figure S17. Rate of O_2 evolution by with respect to $[Ru^{II}(NCN\text{-}Me)(bpy)(OH_2)]^{2+}$ (**1**) in pH~1 triflic acid and 100 mM of CAN.

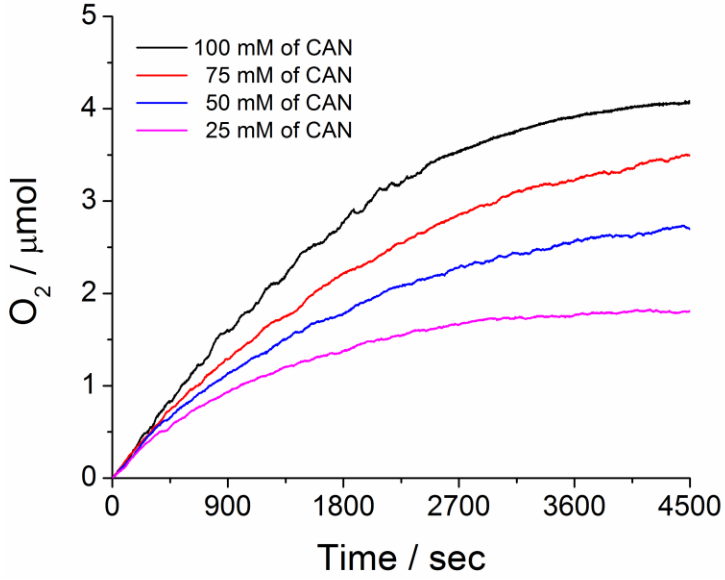

Figure S18. O_2 evolution by 1 mM of $[Ru^{II}(NCN\text{-}Me)(bpy)(OH_2)]^{2+}$ (**1**) in pH~1 triflic acid and various concentration of CAN.

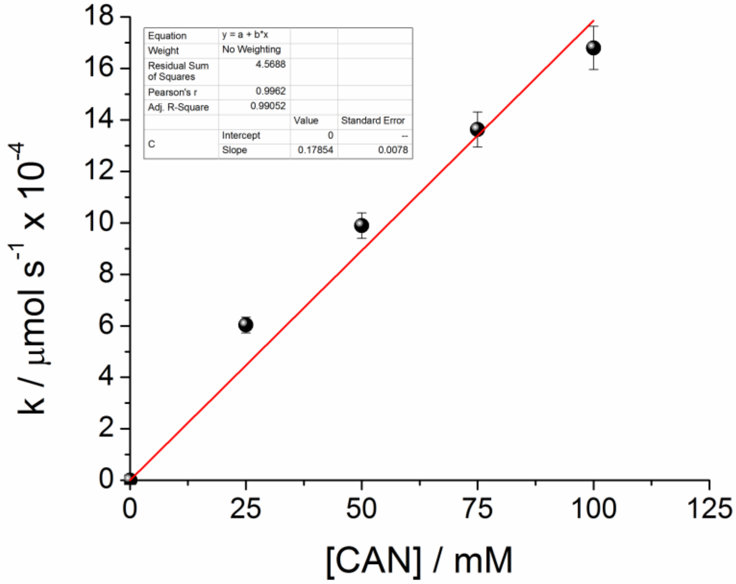

Equation	y = a + b*x		
Weight	No Weighting		
Residual Sum of Squares	4.5688		
Pearson's r	0.9962		
Adj. R-Square	0.99052		
		Value	Standard Error
C	Intercept	0	--
	Slope	0.17854	0.0078

Figure S19. Rate of O_2 evolution by 1 mM $[Ru^{II}(NCN\text{-}Me)(bpy)(OH_2)]^{2+}$ (**1**) in pH~1 triflic acid with respect to various concentration of CAN.

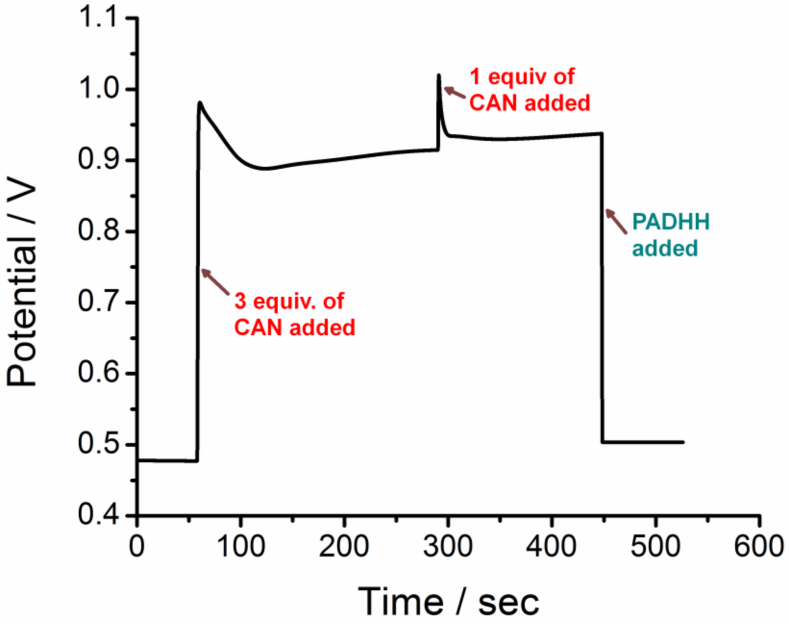

Figure S20. Open circuit potential (OCP) change in $[Ru^{II}(NCN\text{-}Me)(bpy)(OH_2)]^{2+}$ (**1**) at pH~1 triflic acid.

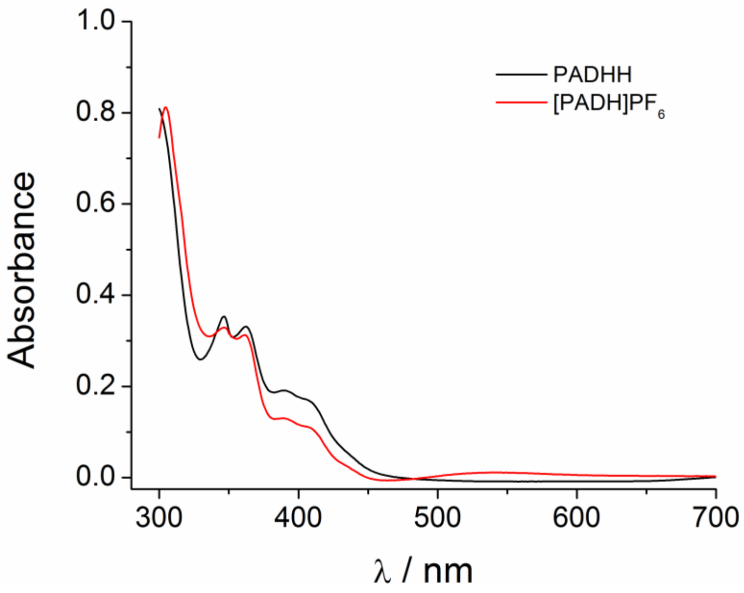

Figure S21. UV-vis spectra of 0.075 mM PADHH and $[PADH]^+PF_6$ in pH~1 HNO_3.

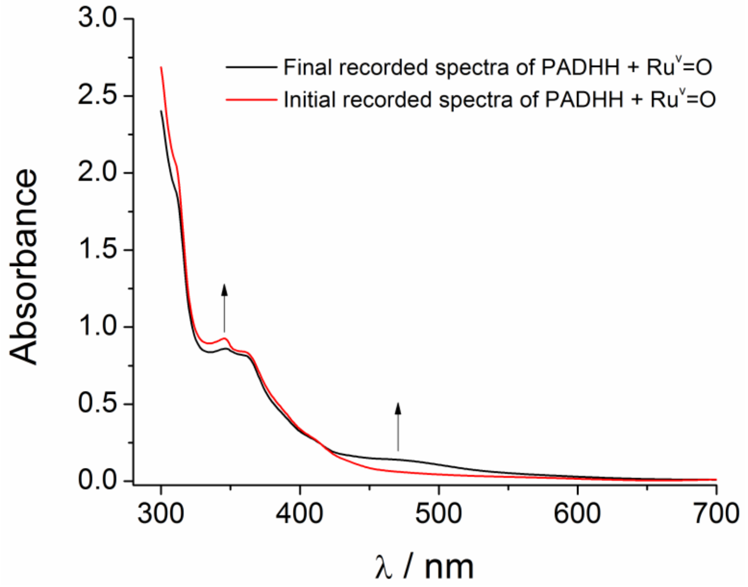

Figure S22. UV-vis spectra of treatment of PADHH and $[Ru^V{=}O]^{3+}$.

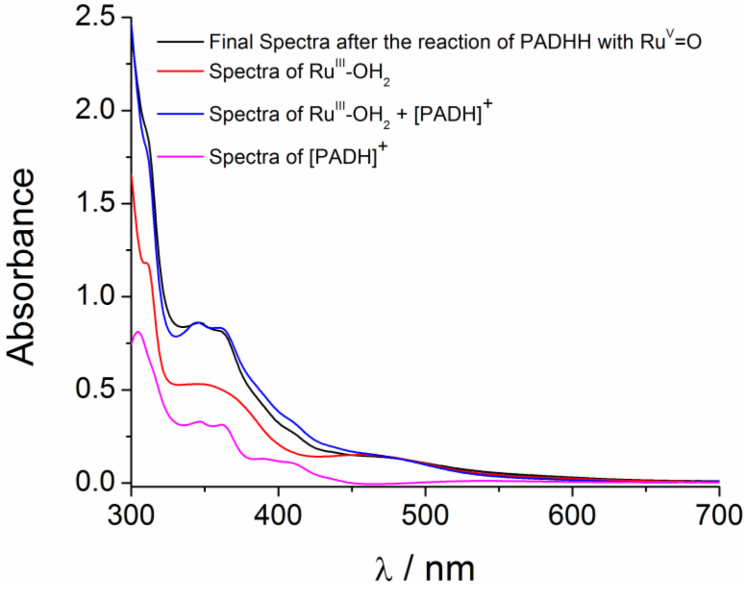

Figure S23. UV-vis spectra of 0.075 mM $[PADH]^+PF_6$ (pink), 0.05 mM $[Ru^{III}(OH_2)]^{3+}$ (red), addition spectra of 0.075 mM $[PADH]^+PF_6$ (pink) and 0.05 mM $[Ru^{III}(OH_2)]^{3+}$ (blue) , final spectra of treatment of 0.075 mM PADHH and 0.05 mM $[Ru^V{=}O]^{3+}$ in pH=1 HNO_3.

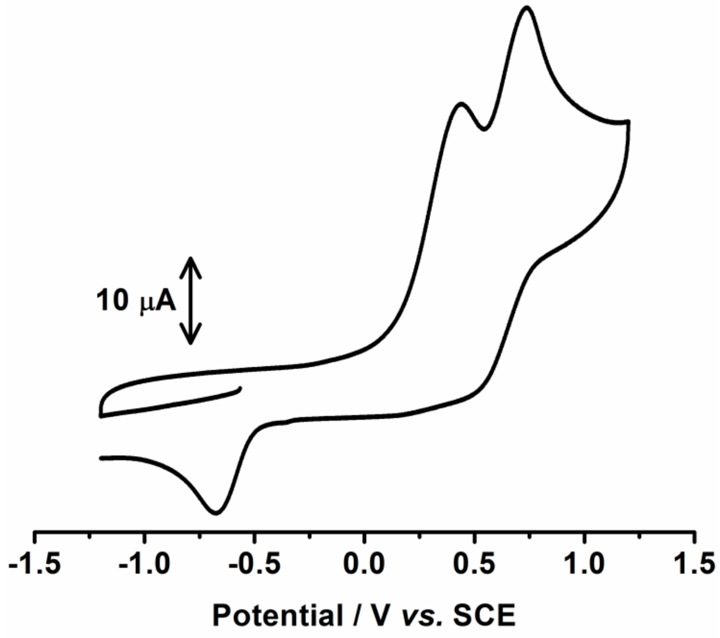

Figure S24. Cyclic voltamogramm of 1 mM PADHH in CH_3CN having 0.1 M Bu_4NPF_6.

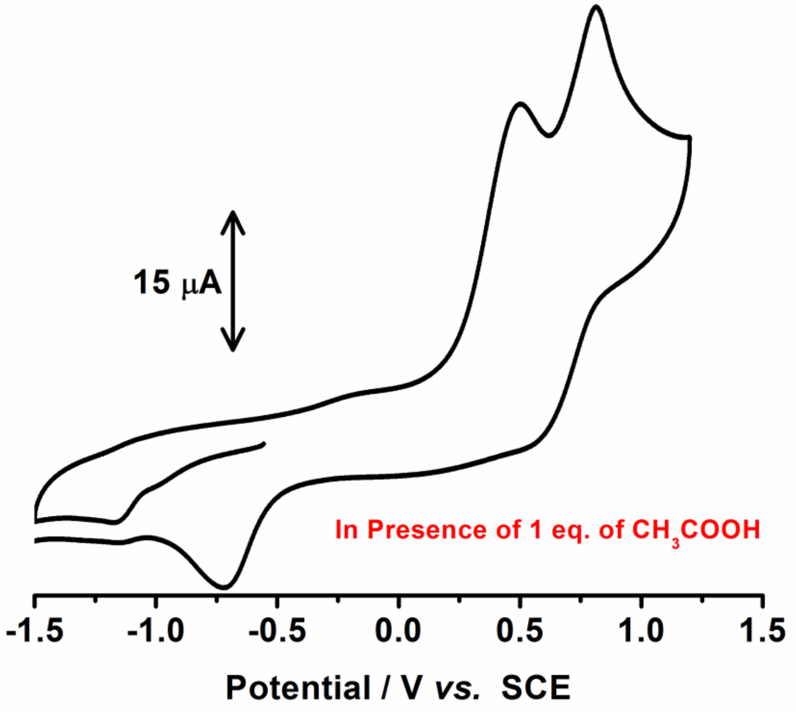

Figure S25. Cyclic voltamogramm of 1 mM PADHH in CH_3CN having 0.1 M Bu_4NPF_6 with the addition of one equivalent of CH_3COOH.

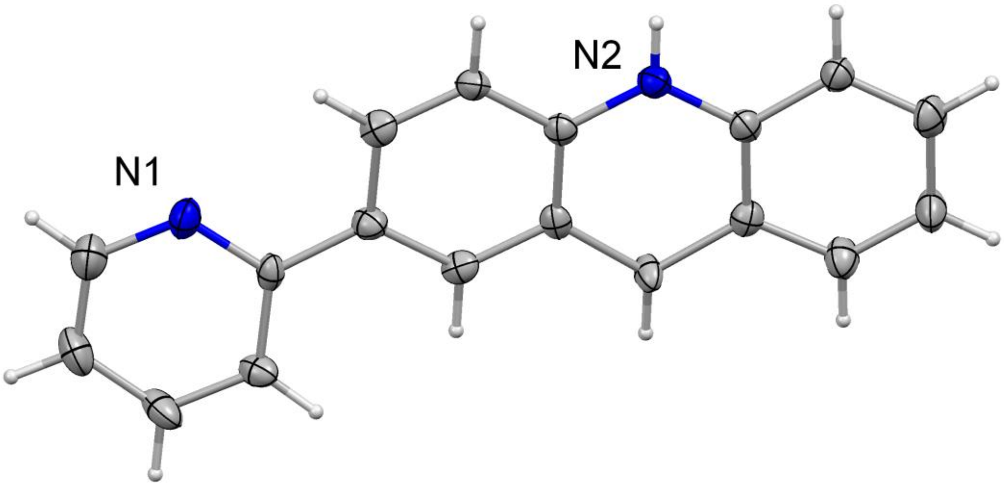

Figure S26. ORTEP (30% probability) of **[PADH]$^+$**.

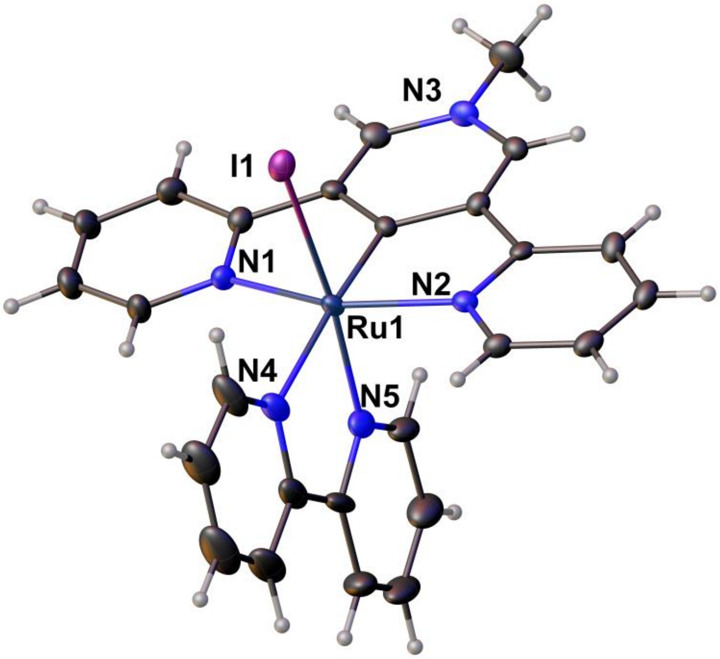

Figure S27. ORTEP (30 %) of [Ru^{II}(NCN-Me)(bpy)(I)]$^+$.

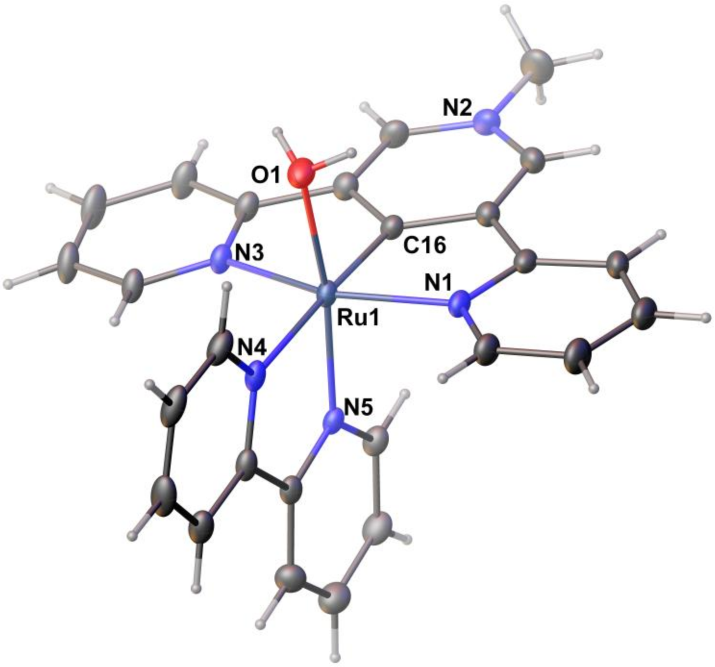

Figure S28. ORTEP (30 %) of $[Ru^{II}(NCN\text{-}Me)(bpy)(OH_2)]^{2+}$.

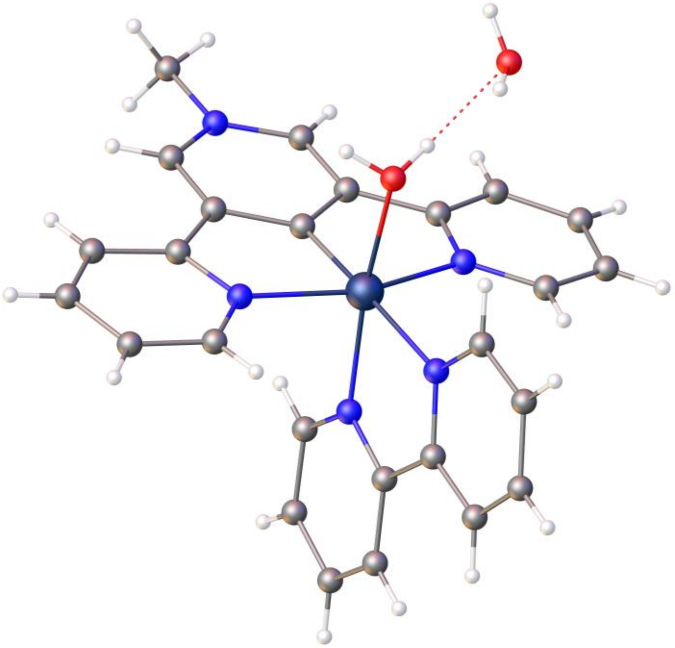

Figure S29. A hydrogen bonded water molecule with the axially coordinated water molecule in $[Ru^{II}(NCN\text{-}Me)(bpy)(OH_2)]^{2+}$.

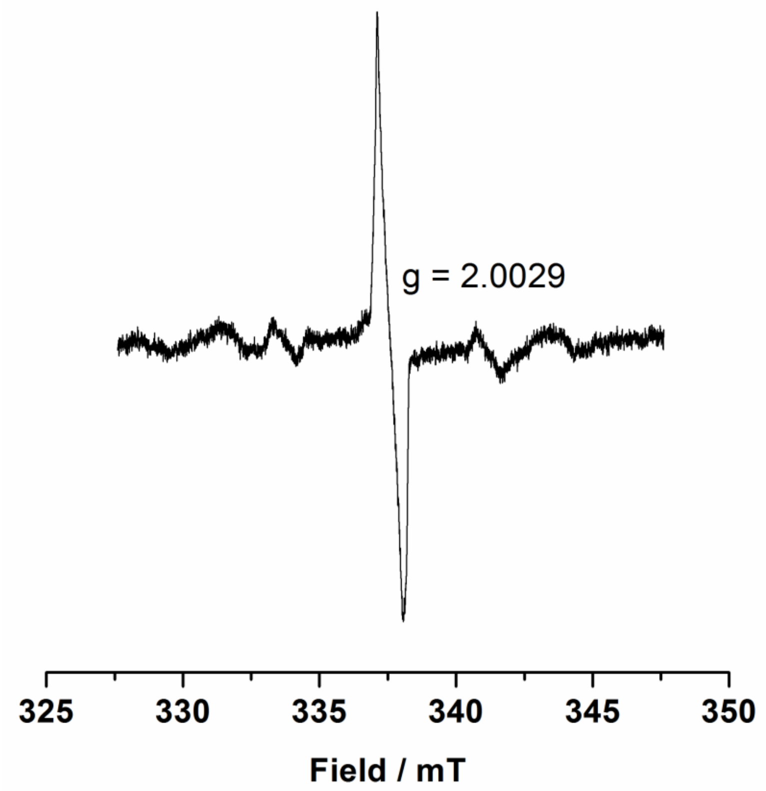

Figure S30. ESR spectrum of PADHH$^{\bullet+}$ in frozen MeCN at 77 K after the addition of $[Ru^{V}=O]^{3+}$ in pH≈1 HNO_3. X-band frquency 9.44 GHz, Microwave power was 1.0 mW and the amplitude was 0.1 mT.

Molecular Structure:

Table S1. Crystal Data and Refinement Parameters

	1	**2**	**$[PADH]^+PF_6$**
Empirical formula	$C_{52}H_{46}F_{18}N_{10}O_{19}P_3Ru_2$	$C_{26}H_{21}F_6IN_5PRu$	$C_{36}H_{26}F_{6.64}N_4P$
CCDC No.	1008770	1008771	1008772
Formula weight	1752.04	776.42	671.78
Temperature (K)	293(2)	298(2)	293(2)
Wavelength, Å	0.71073	0.71073	0.71073
Crystal system	Monoclinic	Monoclinic	Monoclinic
Space group	*C2/c*	*C2/c*	*C2/c*
a, Å	33.819(1)	24.707(2)	15.246(16)
b, Å	14.716(1)	10.320(1)	14.096(12)
c, Å	15.515(1)	24.740(2)	15.181(15)
α, deg			
β, deg	108.58(1)	99.36(1)	119.227(14)
γ, deg			
V, Å^3	7318.5(2)	6224.3(9)	2847(5)
Z	4	8	4
D_{calc} (g cm^{-3})	1.590	1.657	1.567
μ, (mm^{-1})	0.595	1.607	0.177
^{a}GOF on F^2	1.052	1.009	0.916
R [I>2σ(I)]	$^bR_1 = 0.0788$,	$^bR_1 = 0.0681$,	$^bR_1 = 0.0923$,
	$^cwR_2 = 0.1685$	$^cwR_2 = 0.1533$	$^cwR_2 = 0.2398$
R indices (all data)	$^bR_1 = 0.1052$,	$^bR_1 = 0.0689$,	$^bR_1 = 0.1374$,
	$^cwR_2 = 0.2005$	$^cwR_2 = 0.1536$	$^cwR_2 = 0.2686$

^{a}GOF = $[\Sigma[w(F_0^2 - F_c^2)^2]/M - N]^{1/2}$ (M = number of reflections, N = number of parameters refined).^{b}$R_1 = \Sigma ||F_0| - |F_c||/\Sigma|F_0|$.^{c}$wR_2 = [\Sigma[w(F_0^2 - F_c^2)^2]/ \Sigma[w(F_0^2)^2]]$.

References:

(1) G.M. Sheldrick, SADABS, University of Göttingen, Göttingen, Germany, 1996.

(2) (a) SMART and SAINT, Siemens Analytical X-ray Instruments Inc., Madison, WI, 1996. (b) G.M. Sheldrick, SHELXS-97 and SHELXL-97, University of Göttingen, Göttingen, Germany, 1997.